Int J Adv Manuf Technol (2018) 98:119–127
DOI 10.1007/s00170-017-0451-6

ORIGINAL ARTICLE

Serrated chip formation mechanism analysis for machining of titanium alloy Ti-6Al-4V based on thermal property

Jian Zang[1] · **Jun Zhao**[1] · **Anhai Li**[1] · **Jiming Pang**[1]

Received: 12 December 2016 / Accepted: 24 April 2017 / Published online: 26 May 2017
© Springer-Verlag London 2017

Abstract Based on the software ABAQUS/Explicit, a finite element (FE) model for orthogonal cutting was established. The FE model was validated by comparing the cutting forces and serrated degree of chips obtained by orthogonal cutting experiments under the cutting speeds 40, 80, 120, and 160 m/min. Based on the developed FE model, the influence of thermal conductivity on the degree of chip segmentation and the adiabatic shear localization were investigated. Furthermore, the plot contours on undeformed shape of cutting simulation was used to investigate the temperature distribution, and the high temperature zone was identified, which can help enhance the understanding of the serrated chip formation. Finally, cracks located in the adjacent segments of chips were observed. The results show that with the increase in thermal conductivity, the degree of adiabatic shear decreases. It can be concluded that the poor thermal conduction performance should be primarily responsible for the formation of serrated chips during machining Ti-6Al-4V alloy. Due to the high temperature at contact surface between cutting tool and workpiece, the increasing of cutting speed facilitates the formation of serrated chips during machining.

✉ Anhai Li
anhaili@sdu.edu.cn

Jun Zhao
zhaojun@sdu.edu.cn

[1] Key Laboratory of High-efficiency and Clean Mechanical Manufacture of MOE, School of Mechanical Engineering, Shandong University, 17923 Jingshi Road, Jinan 250061, People's Republic of China

Keywords Titanium alloy Ti-6Al-4V · Thermal conductivity · Serrated chips · Chip formation mechanism · Finite element simulation

1 Introduction

High speed machining has been widely employed in industries and aerospace. There are many advantages in high speed machining such as excellent surface quality, low cost, high machining efficiency, and low cutting force [1–3]. There are several differences between high speed machining and conventional speed machining in some aspects in terms of chip formation mechanisms, distribution of cutting temperature, and variations of cutting force.

Titanium alloy Ti-6Al-4V possesses high specific strength, high temperature resistance, and high toughness. Based on these excellent properties, Ti-6Al-4V can maintain enough strength and support greater loading at high temperature [4]. Due to the surface quality have effects on lifespan of material and frictional behavior, the surface machining process is a very important step in manufacturing product. However, the utilization of titanium alloys is restricted by their poor machinability. Many researchers have paid more attention to the investigations on machining mechanism of titanium alloys, including chip formation mechanisms, distribution of temperature, and variations of cutting force, etc. [5, 6]. Due to the unique properties of titanium alloys, especially for their poor thermal property, the chips produced are serrated even at low cutting speed, which is distinctly different from other materials. During the metal alloy cutting process, there are four types of metal chips: flow chip, wavy chip, serrated chip, and discontinuous chip. As the chip formation has significant influence on the change of cutting force, the distribution of cutting temperature in addition to the tool failure and tool wear is important to have

deeper insights into the essential factors that control the chip formation mechanism. Many attentions have been paid to the formation mechanisms of serrated chips, which can mainly be summarized as to the adiabatic shear theory [7, 8]. Recht [9] raised the mechanism of "catastrophic adiabatic shear" to explain the appearance of serrated chip. Chen et al. [10] expounded the thermoplastic instability in deformation zones during the cutting process. Shaw et al. [11] illustrated that the emergence of serrated chip in titanium alloys cutting process is mainly due to the interaction between thermal softening effect and strain hardening effect in the shear zone. Other than that, there are many factors contributing to the formation of serrated, Wan and Wang [12] carried out the cutting simulations and experiments to investigate the effects of cutting speeds, they found that the speed is an important parameter for the formation of serrated chips during the cutting process, chip segmentation degree have positive relationship with the cutting speed. Zhu and Sun [13] researched the influence of tool wear on chip formation during Ti-6Al-4V milling and found that degree of serrated increases with the increase of tool wear. The Johnson-Cook constitutive parameters and fracture constants were also investigated on the serrated chip formation [14, 15]. The chip morphologies are investigated by milling Ti-6Al-4V in different cutting conditions [16].

Therefore, the poor thermal property is an important reason for formation of serrated chips, it is essential to study how the thermal property influence the formation of serrated chips during the Ti-6Al-4V cutting. This paper aims to study the morphologies of serrated chips collected under different thermal conductivities in commercial finite element software. Besides, how the poor thermal conductivity of Ti-6Al-4V leads to the formation of serrated chips in dry cutting is investigated. In addition, the chip segmentation degrees under different cutting speeds are investigated.

2 FE modeling of orthogonal cutting

The orthogonal cutting process of titanium alloy Ti-6Al-4V is simulated using the Abaqus/Explicit FE analysis software. The simulation can avoid the material complexities in cutting process, and it is greatly meaningful for deeply comprehending the chip formation mechanisms [17].

As the simulation technology has the characteristics of high efficiency and economic, the experiments are replaced by simulation. The process of production manufacturing can be simulated with more details which are difficult to capture in experiments. Besides, the numerical simulation can be applied to reduce the number of experiments and save the cost. The numerical simulation have been researched on different aspects of machining process [18–20] and made a huge contribution to technology of metal cutting.

2.1 Geometric model of orthogonal cutting

Many cutting researches are based on the two-dimensional (2D) models in finite element software especially in orthogonal cutting. It is very efficient for metal cutting research by simulate the adiabatic shearing at the primary shear zone.

The planar quadrilateral continuum elements (CPE4RT) are used to establish the workpiece model. Besides, CPE4RT have simplified hourglass control features and integration. Because the metal machining is a process of coupled temperature–displacement, it is necessary to set as nodal variables for temperatures and displacements in the Abaqus/Explicit software. Figure 1 illustrates the configuration and boundary conditions in the model. In order to form chips, the element deletion technique is applied to meet the separation of grid cell during the simulation process. The model for orthogonal cutting is shown in Fig. 1. The uncut material thickness ac is 0.1 mm and the rake angle of cutting tool is 0^{o}. In order to eliminate the deformation error of the cutting tool, the cutting tool in the simulation is set as a rigid body.

The direction of cutting speed and displacement boundary conditions in simulation are shown in Fig. 1.

2.2 Constitutive model of material

It is necessary to consider the influence of intense deformation, strain, strain rate, and temperature simulation model [21]. According to Johnson-Cook flow stress model, the material behavior has been summarized as the strain, strain rate, and temperature. As a result, Johnson-Cook law [22] is used in most cutting simulations. The expression of Johnson-Cook law is formed by three parts:

$$\sigma = (A + B\varepsilon^{n})\left(1 + C\ln\frac{\dot{\bar{\varepsilon}}}{\dot{\bar{\varepsilon}}_{0}}\right)\left[1-\left(\frac{T-T_{r}}{T_{m}-T_{r}}\right)^{m}\right] \quad (1)$$

where A, B, C, m, and n are properties of the workpiece material and their specific values are detailed in Table 1. σ is the equivalent stress, T_m is melting temperature, and T_r represents the room temperature (298 K), and $\dot{\bar{\varepsilon}}$ is the reference strain rate.

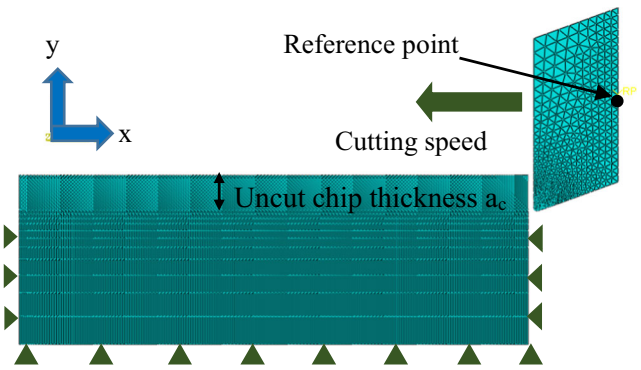

Fig. 1 Orthogonal finite element model

Table 1 The constitutive model parameters of Ti-6Al-4V alloy [23]

A (MPa)	*B* (MPa)	*C*	*n*	*m*
782	498	0.028	0.28	1

The most important advantage of the Johnson-Cook law is the large amount of available parameter for many materials. The physical and mechanical properties value used to describe the Ti-6Al-4V behavior in cutting process are shown in Table 2.

2.3 Chip separation criterion

As the Johnson-Cook fracture model [22] is selected to state the workpiece damage evolution which involves the influence of stress, strain rate, and temperature simultaneously based on the law of cumulative damage described in Eq. (2), the Johnson-Cook fracture is established.

$$w = \sum \frac{\Delta \bar{\varepsilon}}{\bar{\varepsilon}_f} \tag{2}$$

Where w is the damage initiation, $\bar{\varepsilon}_f$ represents the equivalent strain, and $\Delta\bar{\varepsilon}$ represents the incremental value of equivalent plastic strain. The damage evolution of elements is based upon the value of w. The equation of equivalent fracture strain as shown in Eq. (3):

$$\bar{\varepsilon}_f = \left[D_1 + D_2 \exp\left(D_3 \frac{P}{\bar{\sigma}}\right)\right]\left[1 + D_4 \ln\frac{\dot{\bar{\varepsilon}}}{\dot{\bar{\varepsilon}}_0}\right]\left[1 + D_5 \frac{T - T_r}{T_m - T_r}\right] \tag{3}$$

The variables D_1, D_2, D_3, D_4, and D_5 are parameters which describe the failure behavior of material. They respectively represent the factor of the initial failure strain, the exponential triaxiality, the strain rate, and the temperature. The other parameters in Eq. (3) correspond to that in the Johnson-Cook (Eq. (1)) flow law. P indicates hydrostatic pressure and its value equals to an average of three normal stresses. The term $\left[D_1 + D_2 \exp\left(D_3 \frac{P}{\bar{\sigma}}\right)\right]$ indicates the equivalent stain in fracture during the hydrostatic pressure P increases. The ratio of $\frac{P}{\bar{\sigma}}$ is called the stress triaxiality. The variables D_1~D_5 in simulation are presented in Table 3.

During the cutting process in simulation, the damage evolution of element is determined by the value of displacement at failure or fracture energy G_f before the chip forming initiation. Hillerborg [26] proposed the failure criterion of energy-based ductile, which is used to define the damage evolution of material during the process. As a parameter, G_f is applied to produce a unit crack area when chips separate from workpiece. The G_f can be expressed as Eq. (4):

$$G_f = \int_{\bar{\varepsilon}_0}^{\bar{\varepsilon}_f} L\sigma_y d\bar{\varepsilon} = \int_0^{\bar{u}_f} \sigma_y d\bar{u} \tag{4}$$

where $\bar{u}$ is the equivalent plastic deformation. $\bar{\varepsilon}_0$ is the initial plastic strain. According Eq. (5), the damage variable D can be calculated:

$$D = \frac{L\bar{\varepsilon}}{\bar{u}_f} = \frac{\bar{u}}{\bar{u}_f} \tag{5}$$

The grids disappear and the chip generates when D reaches 1.

2.4 Friction and heat generation

The inelastic deformation and friction are important features in the cutting process because it will generate heat and constantly change the material properties. As a result, the research mainly concentrated on the strain, stress in material, and distribution of temperature during the cutting process.

The friction in contact surface of tool-chip is one of the most complex aspects in cutting process, which has serious implications to machining precision and surface quality. The correct relationship between tool and workpiece in simulation is an important factor to simulate the cutting process. So needless to say, that to build a fraction model-involved tool and

Table 2 Mechanical properties of titanium alloy Ti-6Al-4V [24]

Density (kg/m^3)	Elastic modulus (GPa)	Poisson's ratio	Thermal conductivity (W/m·K)	Specific heat (J/kg·K)
4430	109 (50 °C)	0.34	6.8 (20 °C)	611 (20 °C)
	91 (250 °C)		7.4 (100 °C)	624 (100 °C)
	75 (750 °C)		9.8 (300 °C)	674 (300 °C)
			11.8 (500 °C)	703 (500 °C)

Table 3 The fracture constants of JC fracture model for Ti-6Al-4V alloy [25]

D_1	D_2	D_3	D_4	D_5
−0.09	0.25	−0.5	0.014	3.87

workpiece is necessary. Zorev [27] proposed two kinds of contact regions at the interface between the cutting tool and chip: the shear stresses τ_f near the tool tip are regarded as equal to the material shear strength τ_γ. Besides, the stress of friction is proportional to the stress in the normal direction σ_n in the sliding region.

$$\tau_f = \begin{cases} \tau_\gamma, 0 \le l \le L_c \\ \mu\sigma_n, l > L_c \end{cases} \tag{6}$$

where μ represents Coulomb's friction coefficient and L_c is the contact length of transitional contact zone. Similar approaches have been applied to cutting process in simulation.

2.5 Thermal conduction property of the workpiece material

Due to the heat generated from plastic deformation in material and the friction contact between the tool and material during the cutting process, the temperature have a sharp increase in tool tip. On count of temperature difference around tool tip, the heat spread to outside of tip in the form of thermal radiation. The two-dimensional steady-state control equation of thermal conduction:

$$k\left(\frac{\partial^2 T}{\partial^2 x} + \frac{\partial^2 T}{\partial^2 y}\right) + \dot{Q} = \rho C_p \left(u_x \frac{\partial T}{\partial x} + u_y \frac{\partial T}{\partial y}\right) \tag{7}$$

where T is temperature function of x and y in two-dimensional surfaces, k is thermal conductivity, Q is heat flow in unit volume, ρ represents the density of material, C_p is specific heat capacity, u_x, and u_y represent the propagation velocity in x and y direction, respectively.

In the process of cutting, a large amount of plastic strain occurs in workpiece. The heat generated from plastic strain in unit volume:

$$Q_{pl} = \eta \overline{\sigma} \cdot \dot{\varepsilon}_{pl} \tag{8}$$

where η is the ratio that plastic deformation convert to thermal energy, $\eta = 0.9$, $\overline{\sigma}$ is equivalent stress, and ε_{pl} is plastic strain rate.

The heat generated from friction:

$$Q_{fr} = \tau \cdot \dot{\gamma} \tag{9}$$

where τ is shearing stress in tool-chip contacting surface and γ is relative speed of contacting surface.

3 Validation of the finite element model

This section is aim to verify the simulation model of cutting Ti-6Al-4V by the orthogonal cutting experiments. Figure 2 shows the specific setup of experiment. The experiments were carried out on CKD6143H using the PCD TiAlN coating tools (insert type: NG3156R, coated type: KC5025) with a rake angle of zero. The workpiece is unprocessed, which cutting width and slots are also shown in Fig. 2. Due to the width of cutting edge is 3 mm, the slots designed into 3 mm can better avoid impact during the cutting process. The feed rate keep unchanged in all experiment at a value of 0.1 mm/r (equal to ac in FE model), and the cutting speeds are 40, 80, 120, and 160 m/min under dry cutting conditions. The insert was replaced by a new one after each cutting process so as to avoid the errors generated from tool wear.

The chips collected at each end of cutting process were inlaid into mosaic materials under the temperature of 140 °C. After ground and etched, the mosaic specimens can be observed using scanning electron microscope.

For the purpose of verifying the correctness of the simulation model, the degree of chip segmentation G_s defined by Eq. (7) under different cutting speeds are analyzed.

$$G_s = \frac{H - C}{H} \tag{10}$$

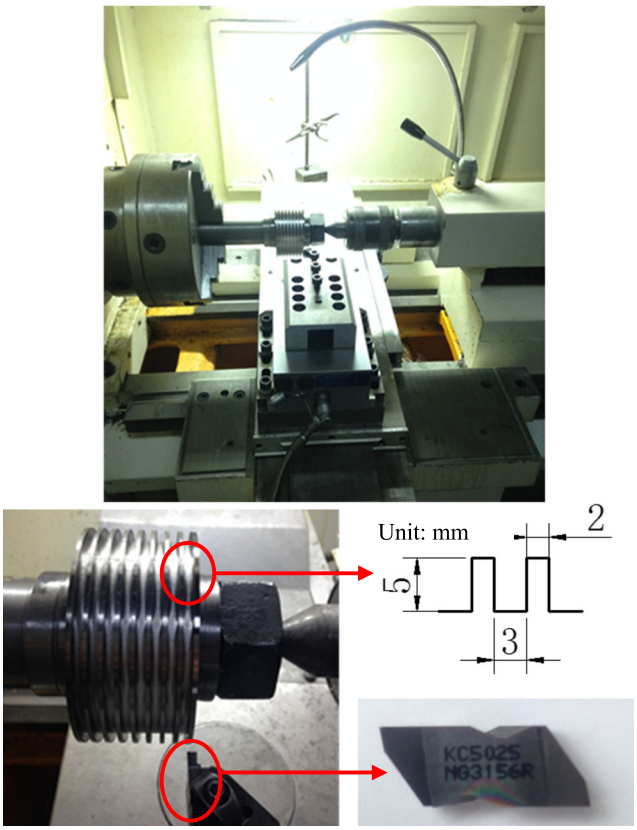

Fig. 2 The equipment for orthogonal cutting

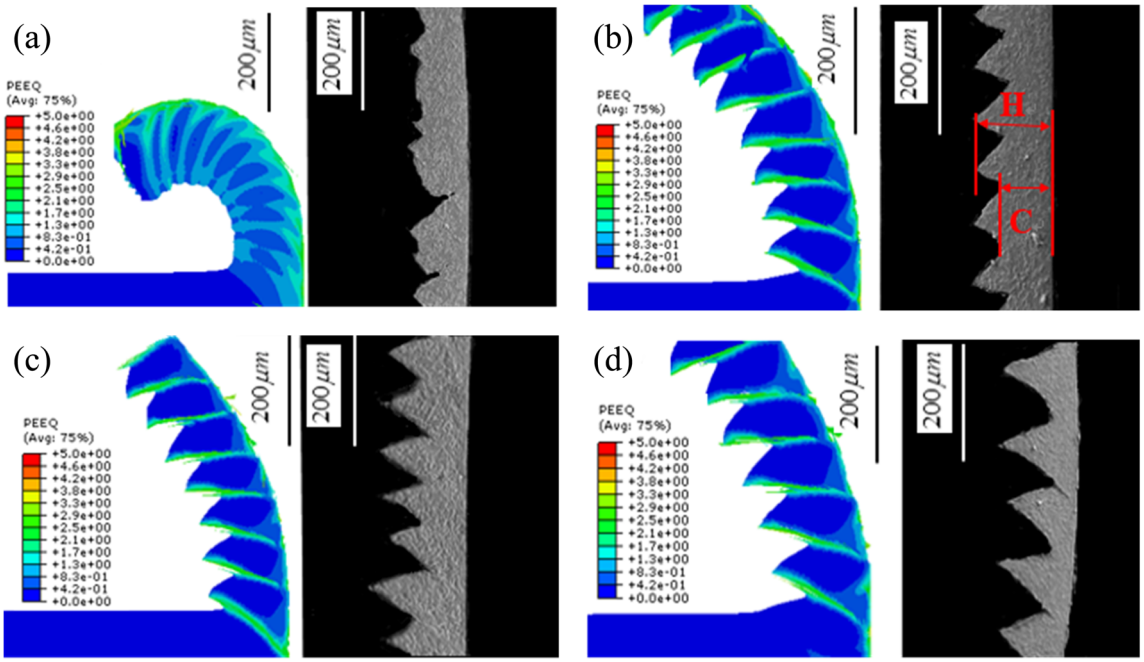

Fig. 3 Comparison of simulated and experimental chips. **a** 40, **b** 80, **c** 120, and **d** 160 m/min

Figure 3 shows the chip morphology obtained in simulation and experiment under different cutting speeds, the H and C represent the values of peak and valley of chip, respectively. The chip morphology of simulation has a good agreement with experimental results.

The chip segmentation degrees G_s of simulation and experimental results are presented in Fig. 4. It can be found that chip segmentation degree G_s has positive correlation with the cutting speed.

Figure 5 shows the cutting forces of simulation and experiment at cutting speeds 40, 80, 120, and 160 m/min, respectively. From the figures, it can be found that the experimental cutting force approximately equals that of simulation at 40 m/min. On the contrary, the cutting forces of experiment are larger than those of simulation at the cutting speeds 80, 120, 160 m/min. Due to the measuring errors of experimental setups, tool wear, and vibration of machine system during the cutting process, a certain error occurred between experiments and simulation. The tool wear is slower under low cutting speeds. As a result, the experimental cutting force approximately equals that of simulation.

In addition, the largest cutting force appear at 120 m/min when the cutting speed ranged from 40 to 120 m/min, then, the cutting force have a reduction when the cutting speed larger than 120 m/min.

According to Figs. 3, 4, and 5, it can be deduced that the results of simulation are coincident well with experiment.

4 Influence of thermal conductivity in adiabatic shear

The poor thermal property of Ti-6Al-4V is the key of emergence of serrated chips, so it is important to study how the thermal property influences the formation of serrated chips. The finite element method is used to study the influence of thermal conductivity in producing serrated chips, and the reasons are as follows: Firstly, considering that metal cutting

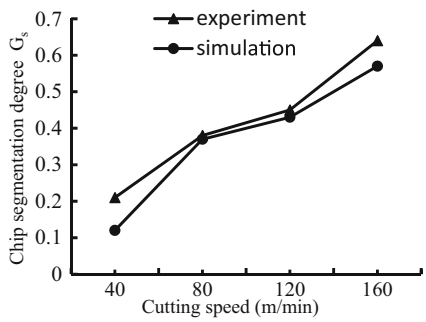

Fig. 4 Variation of chip segmentation degree under different cutting speeds

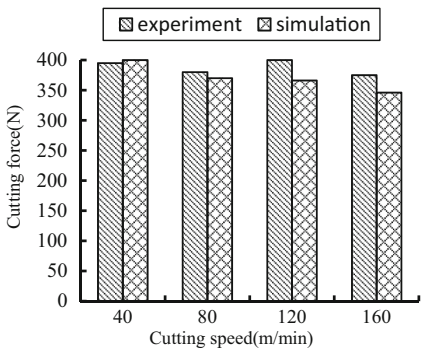

Fig. 5 Average cutting forces under different cutting speeds

Table 4 The selected thermal conductivity in simulation for Ti-6Al-4V

Thermal conductivity (W/m·K)	$k = 0.1\ k_0$	$k = 0.5\ k_0$	$k = k_0$	$k = 1.5\ k_0$	$k = 2\ k_0$
20 °C	0.68	3.4	6.8	10.2	13.6
100 °C	0.74	3.7	7.4	11.1	14.8
300 °C	0.98	4.9	9.8	14.7	19.6
500 °C	1.18	5.9	11.8	17.7	23.6

process is a complicated dynamic process, it is very hard to get the chip temperature distribution during the cutting process; secondly, the flexibility of finite element software can meet the demand to study the chip formation mechanism by varying the thermal conductivity.

In order to research the influence of thermal conductivity in adiabatic shear and to prove the poor heat conduction performance of Ti-6Al-4V titanium alloy is an important reason for producing serrated chips in the cutting process, the coefficient of thermal conductivity is changed, and Table 4 shows the selected values of thermal conductivity in this study. During the cutting simulations, all the parameters of Ti-6Al-4V alloy remain constant except for the thermal conductivity.

Figure 6 presents the chip morphologies obtained from the simulation results under different thermal conductivities. Compared with the simulation as shown, the most obvious characteristic of simulation results is that the chip morphology varies from serrated chips to continuous chip. In addition, the increasing of thermal conductivities increases the diffusion velocity of heat accumulating near the tool tip of the material, alleviates effect of thermal softening, and then the hardening effects of

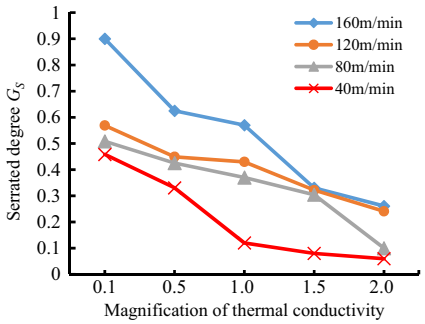

Fig. 7 Chip segmentation degree G_s under different thermal conductivities

strain and strain rate are stronger than thermal softening, so the chip morphology changes from serrated to continuous.

Figure 7 lists chip segmentation degree G_s under different coefficient of thermal conductivity at 40, 80, 120, and 160 m/min, respectively. It can be seen that chip segmentation degree has negative correlations with magnification of thermal conductivity. Combined with the analysis of Fig. 6, it can be deduced that when the thermal conductivity promoting, the heat produced in cutting process can transfer faster to the surrounding material, decreasing the heat aggregation degree round the tool tip, so the thermal softening recede.

As a result, the increase of thermal conductivity decreases the degree of adiabatic shear and the chip segmentation degree. Moreover, the chip segmentation degree has a positive correlation with cutting speed in a same value of thermal conductivity as shown in Fig. 7. The increasing of cutting speed facilitates the process of adiabatic shear localization and the chip segmentation degree of the machined chips.

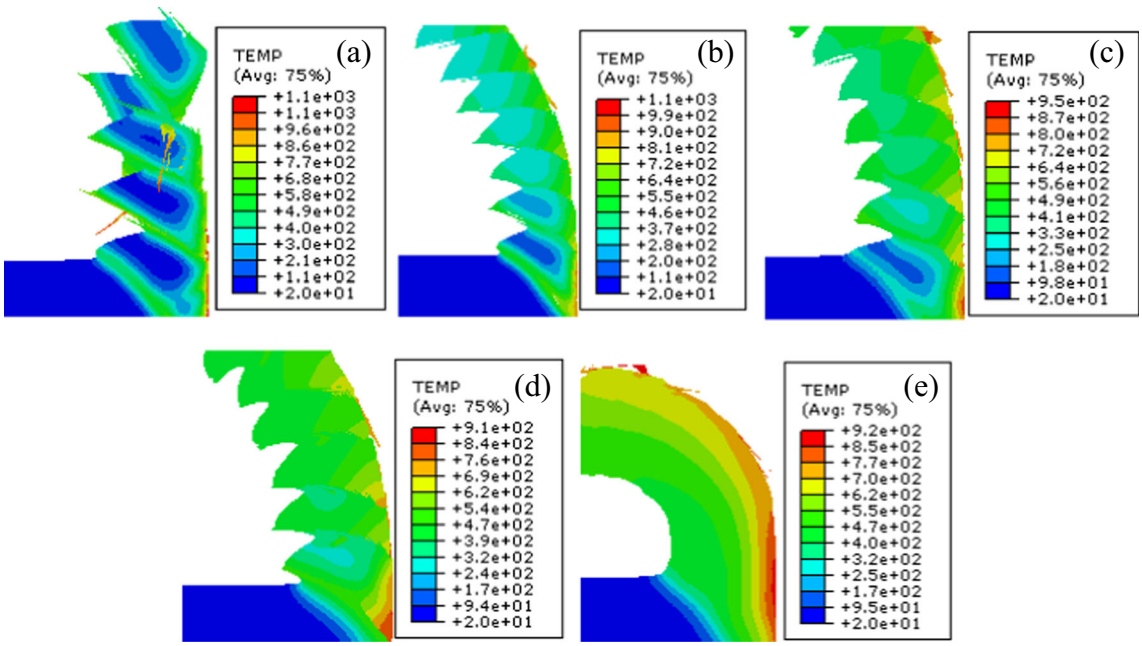

Fig. 6 Variation of chip morphologies under different thermal conductivities when cutting speed is 80 m/min. **a** $k = 0.1\ k_0$; **b** $k = 0.5\ k_0$; **c** $k = k_0$; **d** $k = 1.5\ k_0$; **e** $k = 2\ k_0$

Figure 8 exhibits a series of temperature distribution in the plot contours on undeformed shape of material under the cutting speed 80 m/min, and the chip segments under each magnification of thermal conductivity are detailed. As shown in the figures, the temperatures in the tool-chip interface zones decrease with the increase of thermal conductivity and are greater than other parts of the material. During the heat transfer process, the distribution of temperature should be a continuous change, as shown in Fig. 8e. However, there are high temperature zones in Fig. 8a–d. The reason for this phenomenon is that the thermal softening occurs at the primary shear zone. Meanwhile, under the action of cutting tool, the material of primary shear zone undergoing large deformation, more heat is produced in the high temperature zone. It makes material softening and deformation promote to

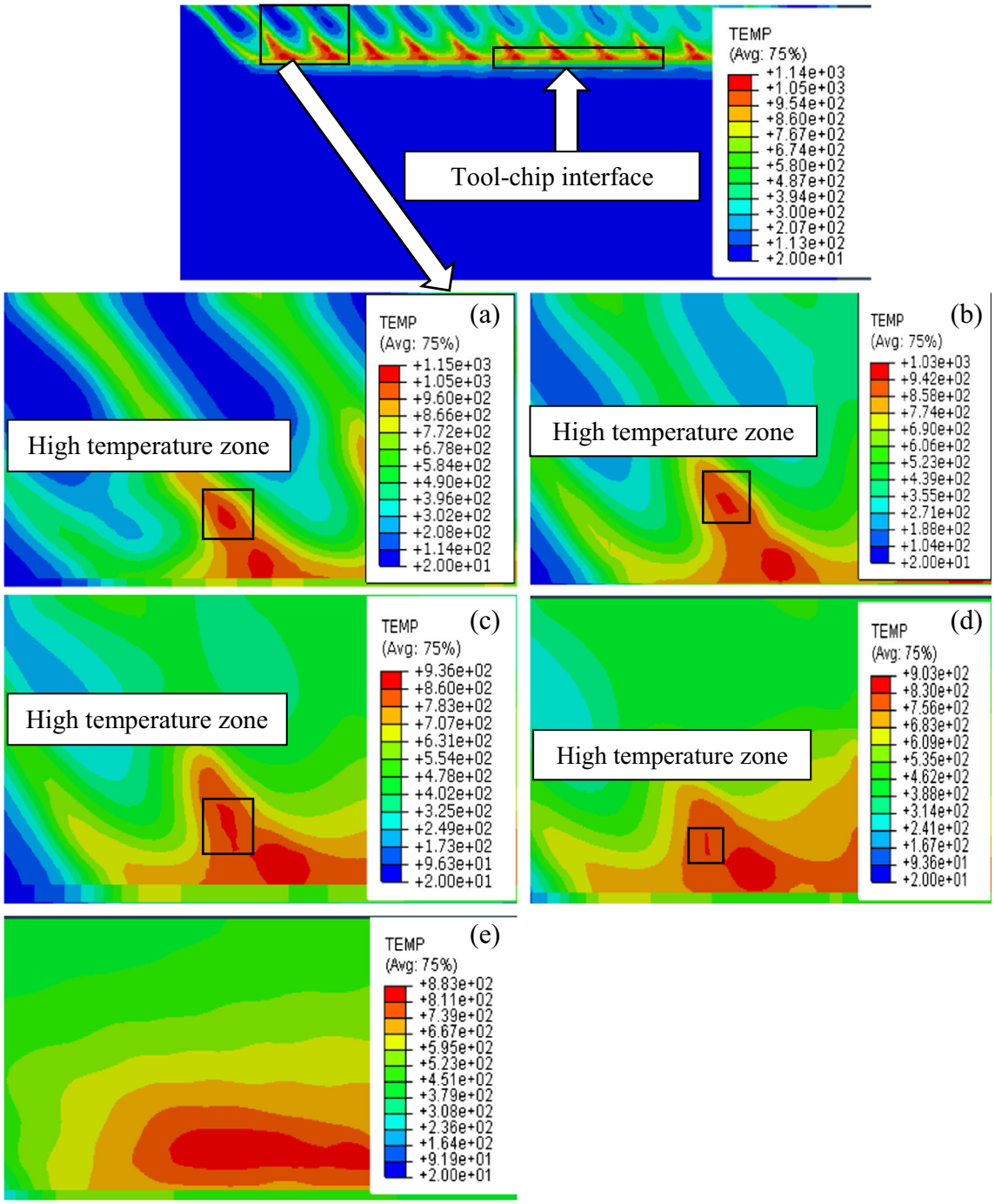

Fig. 8 Temperature distribution in the plot contours on undeformed shape under different thermal conductivities when v is 80 m/min. **a** $k = 0.1\ k_0$; **b** $k = 0.5\ k_0$; **c** $k = k_0$; **d** $k = 1.5\ k_0$; **e** $k = 2\ k_0$

develop mutually. Therefore, the degree of adiabatic shear in the primary shear zone decreases with the increase of the magnification of thermal conductivity.

Besides, as the thermal conductivity increases, the diffusion velocity of heat which generated in the primary deformation zone increases. It can be easily observed in Fig. 8 that the area of high temperature zone is smaller than that of Fig. 8a–c. As shown in Fig. 8e, when the thermal conductivity is $k = 2\ k_0$, the high temperature zone disappears. As a result, with the high temperature zone fades out, the chip morphologies change from serrated to continuous as shown in Fig. 6.

Figure 9 reflects the cross-section of serrated chips and the temperature profiles of adiabatic shear bands for Ti-6Al-4V workpiece material under 80, 120, and 160 m/min, respectively. It can be found that the serrated chips were formed. As shown in the temperature profiles of adiabatic shear bands, the temperature distribution of chip segmentation can be extracted from the plot contours on undeformed shape during the cutting process of simulation and the temperature of adiabatic shear zone is obviously higher than the surrounding region. In addition, the adiabatic shear band and the cracks located in adjacent segment were observed in the micrographs. Indeed, the shear zone initiates around the tool tip and propagates toward the free surface, and then the crack initiates from the free surface of the chip. Furthermore, with the cutting speed increases, the chip-serrated degree G_s and crack length is increasing.

In the cutting process, the temperature in the area near the tool tip is higher than that of free surface of chip because of the friction between the tool and material. Besides, the thermal softening is more apparent in the zone near the tool tip. Therefore, the crack initiates from the free surface of the chip. In addition, when the cutting speed increases, more heat produced resulting from the friction contact between tool and workpiece, leading to the increasing of the degree of adiabatic shear and crack length.

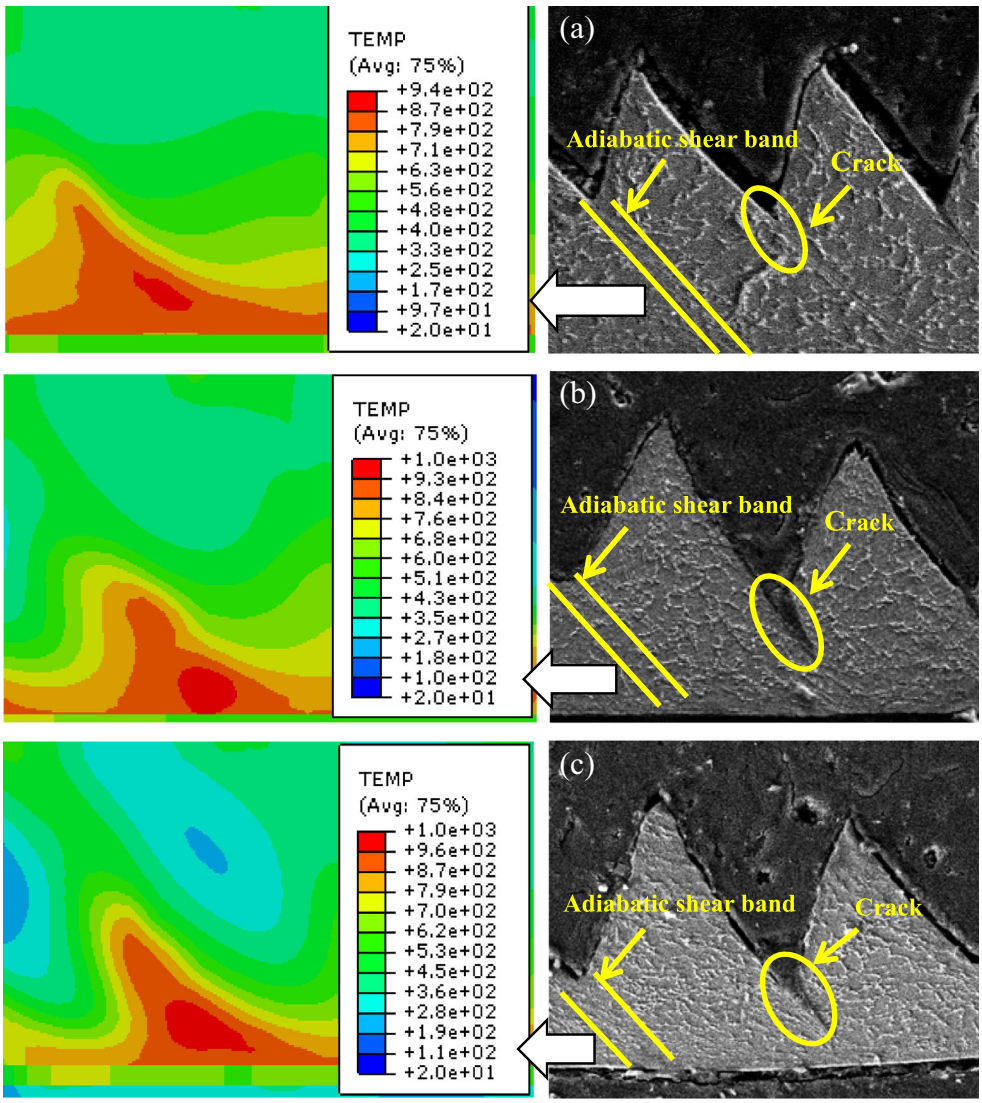

Fig. 9 Micrographs of serrated chips and the temperature profiles of adiabatic shear bands for Ti-6Al-4V **a** 80, **b** 120, and **c** 160 m/min

5 Conclusions

A two-dimensional (2D) model was established based on the finite element software platform. The finite element model is validated by comparing the simulated results with cutting forces and chip segmentation degrees obtained by the cutting experiments. Based on the developed finite element model, the effect of the thermal conductivity of Ti-6Al-4V titanium alloy on the adiabatic shear and chip segmentation was investigated. The crack in the chips was also investigated. The conclusions are drawn as follows:

(1). Based on the results of simulation and experiment, it can be found that the chip segmentation degree G_s has positive correlation with the cutting speed. Besides, the largest cutting force appears at 120 m/min. When the cutting speed is larger than 120 m/min, the cutting force has a decreasing tendency.

(2). The results of simulation show that the serrated degree G_s decreases with the increasing of thermal conductivity. It proves that the poor thermal conduction performance of Ti-6Al-4V titanium alloy is an important reason for the occurrence of serrated chips in the cutting process.

(3). The high temperature zone is identified, which can better explain the adiabatic shear appearing in the primary deformation zone. Furthermore, the high temperature zone illustrates that the adiabatic shear is the result of mutual promotion between material softening and deformation.

(4). The temperature of adiabatic shear zone is obviously higher than the surrounding region during the cutting process and the length of crack located in adjacent of segment has positive correlation with cutting speed.

Acknowledgements This paper is supported by the National Natural Science Foundation of China (51605260, 51475273). The authors would also like to thank the financial support of the China Scholarship Council (CSC).

References

1. Zhang XP, Wu SB (2016) Chip control in the dry machining of hardened AISI 1045 steel. Int J Adv Manuf Technol doi. doi:10.1007/s00170-016-8989-2
2. Ekinovic S, Dolinsek S, Jawahir IS (2004) Some observations of the chip formation process and the white layer formation in high speed milling of hardened steel. Mach Sci Technol 8(2):327–340
3. Pawade RS, Joshi SS, Brahmankar PK (2008) Effect of machining parameters and cutting edge geometry on surface integrity of high-speed turned Inconel 718. Int J Mach Tools Manuf 48(1):15–28
4. Niu W, Bermingham MJ, Baburamani PS, Palanisamy S, Dargusch MS, Turk S, Grigson B, Sharp PK (2013) The effect of cutting speed and heat treatment on the fatigue life of Grade 5 and Grade 23 Ti–6Al–4V alloys. Mater Design 46:640–644
5. Molinari A, Soldani X, Miguélez MH (2013) Adiabatic shear banding and scaling laws in chip formation with application to cutting of Ti–6Al–4V. J Mech Phys Solids 61(11):2331–2359
6. Ginting A, Nouari M (2009) Surface integrity of dry machined titanium alloys. Int J Mach Tools Manuf 49(3):325–332
7. Bakkal M, Shih AJ, Scattergood RO (2004) Chip formation, cutting forces, and tool wear in turning of Zr-based bulk metallic glass. Int J Mach Tools Manuf 44(9):915–925
8. Sutter G (2005) Chip geometries during high-speed machining for orthogonal cutting conditions. Int J Mach Tools Manuf 45(6):719–726
9. Recht RF (1964) Catastrophic thermoplastic shear. J Applied Mechanics 31(2):189–193
10. Chen G, Ren C, Yang X, Tao G (2011) Evidence of thermoplastic instability about segmented chip formation process for Ti–6Al–4V alloy based on the finite-element method. Proc the Inst Mech Eng, Part C: J Mech Eng Sci 225(6):1407–1417
11. Shaw MC, Dirke SO, Smith PA, Cook NH, Loewen EG, Yang CT (1954) Machining titanium. Massachusetts Inst of Tech Cambridge, Dept of Mech Eng
12. Wan L, Wang D, Gao Y (2016) The investigation of mechanism of serrated chip formation under different cutting speeds. Int J Adv Manuf Technol 82(5–8):951–959
13. Zhu Z, Sun J, Li J, Huang P (2016) Investigation on the influence of tool wear upon chip morphology in end milling titanium alloy Ti6Al4V. Int J Adv Manuf Technol 83(9–12):1477–1485
14. Wang B, Liu Z (2014) Investigations on the chip formation mechanism and shear localization sensitivity of high-speed machining Ti6Al4V. Int J Adv Manuf Technol 75(5–8):1065–1076
15. Wang B, Liu Z (2015) Shear localization sensitivity analysis for Johnson–Cook constitutive parameters on serrated chips in high speed machining of Ti6Al4V. Simul Model Pract Theory 55:63–76
16. Li A, Zhao J, Zhou Y, Chen X, Wang D (2012) Experimental investigation on chip morphologies in high-speed dry milling of titanium alloy Ti-6Al-4V. Int J Adv Manuf Technol 62(9–12):933–942
17. Molinari A, Cheriguene R, Miguelez H (2012) Contact variables and thermal effects at the tool–chip interface in orthogonal cutting. Int J Solids Struct 49(26):3774–3796
18. Childs THC (2006) Friction modelling in metal cutting. Wear 260(3):310–318
19. Dixit US, Joshi SN, Davim JP (2011) Incorporation of material behavior in modeling of metal forming and machining processes: a review. Mater Design 32(7):3655–3670
20. Muñoz-Sánchez A, Canteli JA, Cantero JL, Miguélez MH (2011) Numerical analysis of the tool wear effect in the machining induced residual stresses. Simul Model Pract Theory 19(2):872–886
21. Johnson GR, Cook WH (1985) Fracture characteristics of three metals subjected to various strains, strain rates, temperatures and pressures. Eng Fract Mech 21(1):31–48
22. Johnson GR, Cook WH (1983) A constitutive model and data for metals subjected to large strains, high strain rates and high temperatures. In: Proc 7th Int Symp Ballist 21: 541-547
23. Lee WS, Lin CF (1998) High-temperature deformation behavior of Ti6Al4V alloy evaluated by high strain-rate compression tests. J Mater Process Technol 75(1):127–136
24. Chen G, Ren C, Yang X, Jin X, Guo T (2011) Finite element simulation of high-speed machining of titanium alloy (Ti-6Al-4V) based on ductile failure model. Int J Adv Manuf Technol 56(9–12):1027–1038
25. Davies MA, Chou Y, Evans CJ (1996) On chip morphology, tool wear and cutting mechanics in finish hard turning. CIRP Annals-Manuf Technol 45:77–82
26. Hillerborg A, Modéer M, Petersson PE (1976) Analysis of crack formation and crack growth in concrete by means of fracture mechanics and finite elements. Cem Conc Res 6(6):773–781
27. Zorev N (1963) Inter-relationship between shear processes occurring along tool face and shear plane in metal cutting. Int Res Prod Eng 49:143–152